

Geometric control of concurrence and quantum gate operations in triangular triple quantum dots

Junqing Li(李俊青), Shuo Dong(董硕), and Jianhua Wei(魏建华)
Citation: Chin. Phys. B, 2026, 35 (**2**): 020302. DOI: 10.1088/1674-1056/adec5d
http://cpb.iphy.ac.cn; http://iopscience.iop.org/cpb

What follows is a list of articles you may be interested in

A pure quantum secret sharing scheme based on GHZ basis measurement and quantum entanglement exchange

Bai Liu(刘白), Jun Zhang(张俊), Shupin Qiu(邱书品), and Mingwu Zhang(张明武)
Chin. Phys. B, 2025, 34 (**3**): 030304. DOI: 10.1088/1674-1056/ada548

Enhancing entanglement and steering in a hybrid atom-optomechanical system via Duffing nonlinearity

Ling-Hui Dong(董凌晖), Xiao-Jie Wu(武晓捷), Cheng-Hua Bai(白成华), and Shao-Xiong Wu(武少雄)
Chin. Phys. B, 2025, 34 (**2**): 020304. DOI: 10.1088/1674-1056/ad9ba2

Established conversions for hybrid entangled states assisted by error-predicted parity-discriminated devices

Fang-Fang Du(杜芳芳), Zhi-Guo Fan(范志国), Xue-Mei Ren(任雪梅), Ming Ma(马明), and Wen-Yao Liu(刘文耀)
Chin. Phys. B, 2025, 34 (**1**): 010303. DOI: 10.1088/1674-1056/ad8fa0

Generation of macroscopic entanglement in ensemble systems based on silicon vacancy centers

Jian-Zhuang Wu(武建壮), Ying Xi(奚滢), Bo-Ya Li(李博雅), Lian-E Lu(芦连娥), and Yong-Hong Ma(马永红)
Chin. Phys. B, 2024, 33 (**9**): 090308. DOI: 10.1088/1674-1056/ad5d93

Delayed-measurement one-way quantum computing on cloud quantum computer

Zhi-Peng Yang(杨智鹏), Yu-Ran Zhang(张煜然), Fu-Li Li(李福利), and Heng Fan(范桁)
Chin. Phys. B, 2024, 33 (**9**): 090304. DOI: 10.1088/1674-1056/ad6253

Geometric control of concurrence and quantum gate operations in triangular triple quantum dots

Junqing Li(李俊青)[†], Shuo Dong(董硕), and Jianhua Wei(魏建华)[‡]

Department of Physics, Renmin University of China, Beijing 100876, *China*

(Received 6 May 2025; revised manuscript received 7 July 2025; accepted manuscript online 7 July 2025)

As an important index to measure the degree of entanglement in quantum systems, concurrence plays an important role in practical research. In this paper, we study the concurrence between two qubits in triangular triple quantum dot structure. Through calculation and simulation, it is found that concurrence is mainly affected by the interdot coupling strength t, Coulomb interaction U, temperature T, and electrode coupling Γ. Through comparative studies with parallel triple quantum dot structures, we demonstrate that the triangular geometry exhibits significantly enhanced concurrence under identical conditions. In addition, under the condition that concurrence exceeds 0.9, the functional relationship between t and U is obtained through simulation, which provides theoretical support for quantum dot regulation under high entanglement. Finally, we demonstrate the feasibility of implementing a three-qubit quantum gate, using the Toffoli gate as a representative example, under the condition that the triangular triple quantum dot system maintains high entanglement.

Keywords: transition coupling interaction, triangular triple quantum dots, quantum entanglement, Coulomb interaction, quantum computing

PACS: 03.67.Bg, 81.07.Ta, 03.67.Hk, 03.67.Mn, 03.67.Ac

DOI: 10.1088/1674-1056/adec5d **CSTR:** 32038.14.CPB.adec5d

1. Introduction

Concurrence,[1–8] as a fundamental metric in quantum information theory,[9–11] serves as a pivotal quantitative tool for characterizing the entanglement degree of bipartite quantum systems. Its universality and operational significance have established it as an indispensable resource across both theoretical explorations and experimental implementations. Notably, concurrence has found extensive applications in frontier domains, including quantum computing[12–15] (e.g., entangled state preparation and gate fidelity assessment), quantum communication protocols[16–20] (e.g., security analysis of entanglement-based cryptography), and condensed matter physics[21–23] (e.g., quantifying quantum correlations in many-body systems). This measure has become particularly instrumental in bridging abstract entanglement theory with experimentally verifiable quantum phenomena.

In quantum transmission, quantum gates play a key role in the operation and transformation of quantum states, helping to realize information encoding, transmission, error correction and decoding. Especially in quantum communication and quantum networks, quantum gates are essential for the transmission and processing of quantum information to keep the quantum state intact. The Toffoli quantum gate has a unique position among many quantum gates, and its multi-bit control characteristics provide important support for quantum computing and quantum information processing.

In Fig. 1, we give the structure diagram of the triangular three quantum dots. QD1, QD2 and QD3 represent the three quantum dots, t_{12}, t_{13} and t_{23} represent the coupling strength of the tunnel between the quantum dots, QD2 and QD3 are respectively connected to the electrodes Γ.

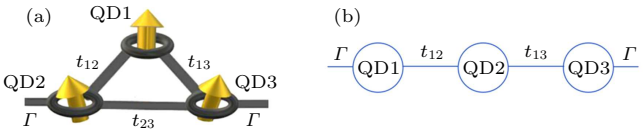


Fig. 1. (a) QD1, QD2 and QD3 represent the three quantum dots, and t_{12}, t_{13} and t_{23} respectively represent the coupling intensity between the quantum dots. The left and right sides of QD2 and QD3 are connected to electrodes Γ, respectively. (b) When the coupling intensity $t_{23} = 0$ meV, we refer to it as parallel triple quantum dot structure.

This paper begins with a comprehensive presentation of the fundamental theoretical framework governing triangular triple quantum dots (TTQDs),[44,45] systematically characterizing the system's critical parameters, including interdot coupling strength t, Coulomb interaction U (in the Hamiltonian, we use U_j to represent Coulomb interaction), temperature T, and electrode coupling Γ. Subsequently, through systematic parameter-space exploration of these variables, we compare the concurrence of the TTQD structure with that of the parallel triple quantum dot structure. Under the same interdot coupling strength, Coulomb interaction, temperature, and electrode coupling, we find that the triangular structure is more likely to maintain a high concurrence. In addition, the function relationship between the interdot coupling strength t, and the

[†]Corresponding author. E-mail: lijunqing@ruc.edu.cn

[‡]Corresponding author. E-mail: wjh@ruc.edu.cn

© 2026 Chinese Physical Society and IOP Publishing Ltd. All rights, including for text and data mining, AI training, and similar technologies, are reserved.

Coulomb interaction U, is obtained by simulation. This quantitatively optimized relationship provides concrete design criteria for maintaining high entanglement (concurrence ≥ 0.9) in practical quantum dot architectures, thereby advancing the engineering of robustly entangled states for quantum information processing applications.

2. Theoretical methods

The TTQD structure is one of the important research directions in the field of quantum dots. In a triangular structure, three quantum dots can form a highly entangled multibody quantum state, and the coupling intensity can be adjusted to achieve precise control of the quantum state. The total Hamiltonian[26–28] for the quantum open system is written as

$$H = H_{\rm dots} + H_{\rm res} + H_{\rm coup}, \tag{1}$$

where $H_{\rm coup}$ represents the coupling Hamiltonian between the electrode and quantum dots, $H_{\rm res}$ and $H_{\rm dots}$ represent the Hamiltonian of the electrode and the Hamiltonian of quantum dots, respectively. The $H_{\rm dots}$ part can be expressed as

$$H_{\rm dots} = \sum_{i=1}^{3} \varepsilon \hat{n}_i + \sum_{j=1}^{3} U_j \hat{n}_{j\uparrow}\hat{n}_{i\downarrow} + \sum_{i,j=1}^{3}\sum_{s=\uparrow,\downarrow} t_{ij}\hat{d}_{is}^{\dagger}\hat{d}_{js}, \tag{2}$$

where ε represents the local energy level of quantum dot, $\hat{n}_i$ represents the number of electrons on QDi, U_j represents the Coulomb interaction of quantum QDj, $\hat{n}_{js} = \hat{d}_{js}^{\dagger}\hat{d}_{js}$ represents the number of electrons with spin s on QDj ($s = \uparrow, \downarrow$), t_{ij} represents the coupling strength between QDi and QDj, $\hat{d}_{is}^{\dagger}$ represents the creation operator for spin s on QDi, and $\hat{d}_{js}$ represents the annihilation operator for spin s on QDj.

The $H_{\rm res}$ and $H_{\rm coup}$ parts of the Hamiltonian are expressed as

$$H_{\rm res} = \sum_{\alpha\in L,R}\sum_{\kappa s}(\varepsilon_{\alpha\kappa s} + \mu_\alpha)\hat{c}_{\alpha\kappa s}^{\dagger}\hat{c}_{\alpha\kappa s}, \tag{3}$$

where $\mu_L = -\mu_R = eV/2$, $\varepsilon_{\alpha\kappa s}$ is the energy of an electron in the α-electrode, κ-momentum and s-spin states, $\hat{c}_{\alpha\kappa s}^{\dagger}$ and $\hat{c}_{\alpha\kappa s}$ are the generation and annihilation operators of electrons in the reservoir, respectively, and the decoherence part of the chiral qubit is mainly defined by this part.

$$H_{\rm coup} = \sum_{\kappa s}(t_{L2}\hat{c}_{L\kappa s}^{\dagger}\hat{d}_{2s} + t_{R3}\hat{c}_{R\kappa s}^{\dagger}\hat{d}_{3s} + \text{H.c.}). \tag{4}$$

The parameters t_{L2} and t_{R3} represent the linear coupling coefficients, where t_{L2} describes the coupling between QD2 and the left electrode, while t_{R3} characterizes the coupling between QD3 and the right electrode.

The hierarchical equations of motion (HEOM)[24] formalism provides a unified framework for investigating quantum dot systems under both equilibrium and nonequilibrium conditions. Rooted in the Feynman–Vernon influence functional path integral approach, this nonperturbative methodology enables rigorous treatment of general quantum systems coupled to fermionic reservoirs obeying Grassmann Gaussian statistics. Particularly noteworthy is the HEOM's ability to deliver numerically exact solutions for complex impurity models, including the challenging three-impurity Anderson system.[25,29–32] Through systematic truncation of the hierarchical expansion governed by convergence criteria, the method achieves high-precision determination of dynamical observables in strongly correlated quantum impurity systems.

The HEOM formalism exhibits several distinctive advantages in quantum impurity system analysis. First, its unified Hamiltonian framework remains structurally invariant across arbitrary parameter regimes eliminating the need for case-specific operator rederivation or computational algorithm redesign. As a nonperturbative approach rooted in open quantum system theory, the HEOM formalism provides rigorous treatment of dissipative dynamics in fermionic reservoirs through its inherent time-nonlocal memory kernel construction. The methodology guarantees formal exactness for noninteracting electron reservoirs while maintaining controlled accuracy for weakly correlated environments through systematic hierarchy truncation. This unique combination of parametric versatility, fundamental exactness, and practical scalability positions the HEOM as an indispensable tool for investigating strongly correlated quantum phase transitions and nonequilibrium transport phenomena.

3. Results and discussion

In a TTQD system, the concurrence[33] between two quantum dots can be expressed as (the detailed derivation process can be found in Appendix A)

$$C_{ij}(t_t) = \max\left\{0, -\frac{1}{2} - 2\frac{S_{ij}(t_t)}{\langle\Psi(t_t)|N_i^s N_j^s|\Psi(t_t)\rangle}\right\}, \tag{5}$$

where $N_i^s = n_{i\uparrow} + n_{i\downarrow} - 2n_{i\uparrow}n_{i\downarrow}$, N_i^s represents the projection operator indicating the presence of a single electron on QDi (i.e., the state where only one electron is occupied), and t_t represents time (in ps), $S_{ij}(t_t) = \langle\Psi(t_t)|\overrightarrow{S_i}\cdot\overrightarrow{S_j}|\Psi(t_t)\rangle$.

To systematically investigate the impact of key physical parameters on quantum entanglement (characterized by concurrence) in the TTQD system and perform a comparative analysis with their parallel counterparts, unlike the TTQD system, the parallel quantum dot system is characterized by an interdot coupling strength of $t_{23} = 0$ meV between QD2 and QD3. We comprehensively examine the roles of critical factors including interdot coupling strength t, Coulomb interaction U, temperature T, and electrode coupling Γ, in both configurations.

As shown in Fig. 2(a), under fixed parameters $T = 0.5$K, electrode coupling $\Gamma = 2.0$ meV, and Coulomb interaction

$U = 0.5$ meV, the concurrence exhibits a monotonic enhancement with increasing interdot coupling strength t, indicating the constructive role of tunnel coupling in quantum correlation formation. Comparative analysis between the TTQD and parallel triple quantum dot configurations under identical t conditions reveals that the TTQD geometry sustains stronger entanglement characteristics. In Fig. 2(b), with fixed $T = 0.5$ K, $\Gamma = 2.0$ meV, $t = 1.0$ meV, the concurrence decreases with the increase of U, and U can inhibit the increase of concurrence. At the same time, we compared the concurrence under the TTQD and the parallel triple quantum dot structure. With the increase of U, the concurrence under the parallel triple quantum dot structure decreased significantly, although the concurrence in the TTQD structure exhibited a downward trend, it remained highly entangled.

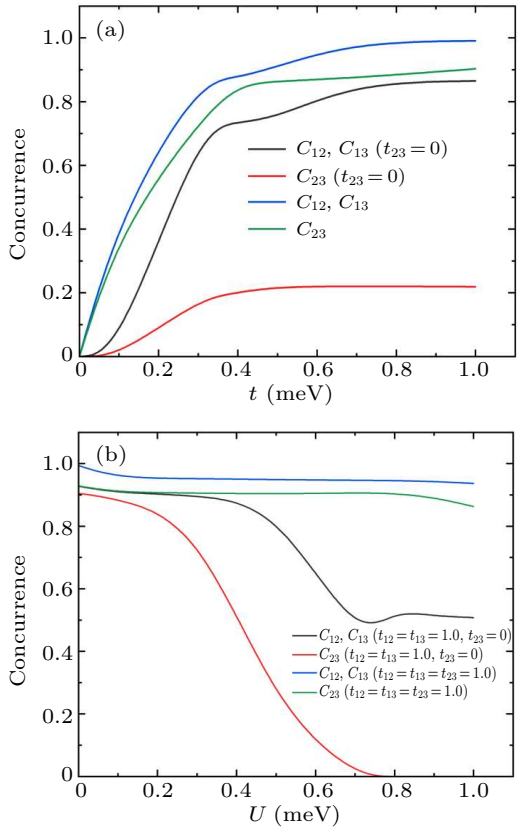


Fig. 2. (a) At temperature $T = 0.5$ K, electrode coupling $\Gamma = 2.0$ meV, Coulomb interaction $U = 0.5$ meV, the concurrence changes with interdot coupling strength. (b) At temperature $T = 0.5$ K, electrode coupling $\Gamma = 2.0$ meV, interdot coupling strength $t = 1.0$ meV, the concurrence changes with the Coulomb interaction U.

In Fig. 3(a), with fixed $T = 0.5$ K, $U = 0.5$ meV, $t = 0.5$ meV, the concurrence increases rapidly with the increase of Γ, and decreases very slowly (negligible) with the continuous increase of Γ. Γ can promote the increase of concurrence. The electrode coupling Γ between the electrode and the quantum dot determines the rate at which electrons tunnel into/out of the quantum dot. Additionally, we compare the concurrence under TTQD and parallel triple quantum dot structures. With the increase of Γ, the concurrence under the parallel triple quantum dot structure cannot reach 0.9. However, the TTQD system exhibits extremely high concurrence.

In Fig. 3(b), with fixed $\Gamma = 2.0$ meV, $U = 0.5$ meV, $t = 0.7$ meV, the concurrence decreases with the increase of T, and T can inhibit the increase of concurrence. We compare the concurrence under the TTQD and parallel triple quantum dot structures. With the increase of T, the concurrence in the parallel triple quantum dot structure is smaller than that in the TTQD structure.

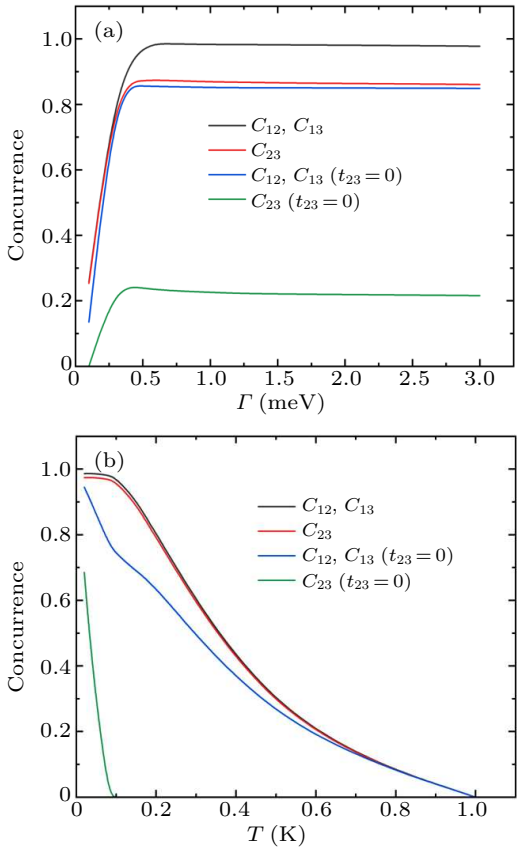


Fig. 3. (a) At temperature $T = 0.5$ K, interdot coupling strength $t = 0.5$ meV, Coulomb interaction $U = 0.5$ meV, the concurrence changes with electrode coupling Γ. (b) At electrode coupling $\Gamma = 2.0$ meV, $U = 0.5$ meV, interdot coupling strength $t = 0.7$ meV, the concurrence changes with temperature T.

Through comparative analysis of the concurrence dependence on interdot coupling strength (t), Coulomb interaction (U), electrode coupling (Γ), and temperature (T) in both triangular (TTQD) and parallel triple quantum dot configurations, we consistently observe significantly higher concurrence values in the TTQD system across all parameter variations. This inherent advantage demonstrates the TTQD architecture's superior potential for experimental quantum applications.

Having established the superior entanglement characteristics of the TTQD configuration compared to its parallel counterpart, we now investigate the parameter space required to maintain high entanglement (concurrence ≥ 0.9). Specifically, under conditions of fixed electrode coupling (Γ) and temperature (T), we examine the optimal regulation.

In Fig. 4(a), with fixed $T = 0.5$ K, $\Gamma = 2.0$ meV, $U = 1.0$ meV, the concurrence with the change of t, we can find from the figure that when $t = 0.4$ meV, the concurrence value can only reach about 0.2. Therefore, when $t = 0.4$ meV, we need to calculate what value U should be adjusted to for the concurrence to reach 0.9. For this reason, we fixed $T = 0.5$ K and $\Gamma = 2.0$ meV in Fig. 4(b). When $t \in (0.3\ \text{meV},\ 0.7\ \text{meV})$, concurrence changes with U.

For example, in Fig. 4(a), when $t = 0.4$ meV, the concurrence value can only reach about 0.2. In this case, when $t = 0.4$ meV in Fig. 4(b) is found, the maximum U value corresponding to concurrence above 0.9 is 0.74.

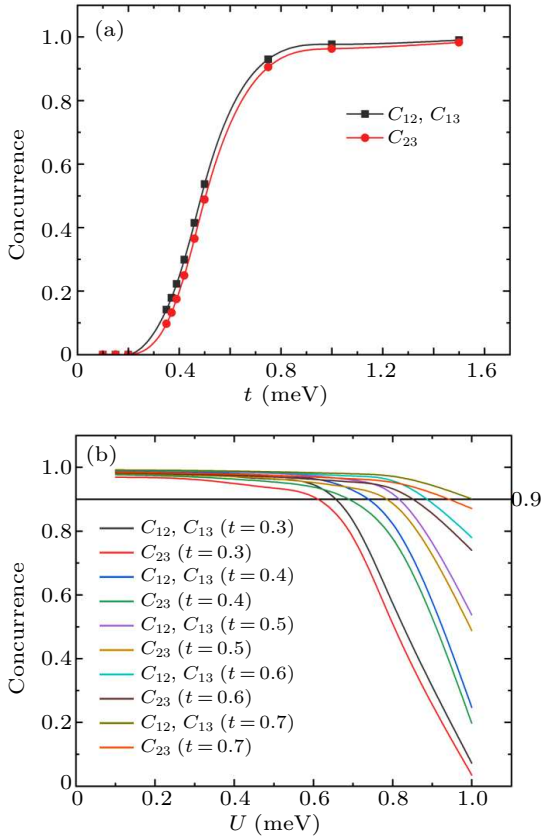


Fig. 4. (a) At temperature $T = 0.5$ K, electrode coupling $\Gamma = 2.0$ meV, Coulomb interaction $U = 1.0$ meV, the concurrence changes with inter-dot coupling strength. (b) At $T = 0.5$ K and $\Gamma = 2.0$ meV, when $t \in$ (0.3 meV–0.7 meV), the concurrence changes with U.

On the premise that the concurrence reaches 0.9, in Fig. 5, we simulate the images of t and U. Through the images, we find that the relationship between t and U is approximately linear, and the correlation function is as follows:

$$C_{12}(C_{13}) : U = 0.82t + 0.41, \tag{6}$$

$$C_{23} : U = 0.79t + 0.379. \tag{7}$$

With the resulting linear function, we can adjust the values of t and U so that the entanglement inside the system is always 0.9.

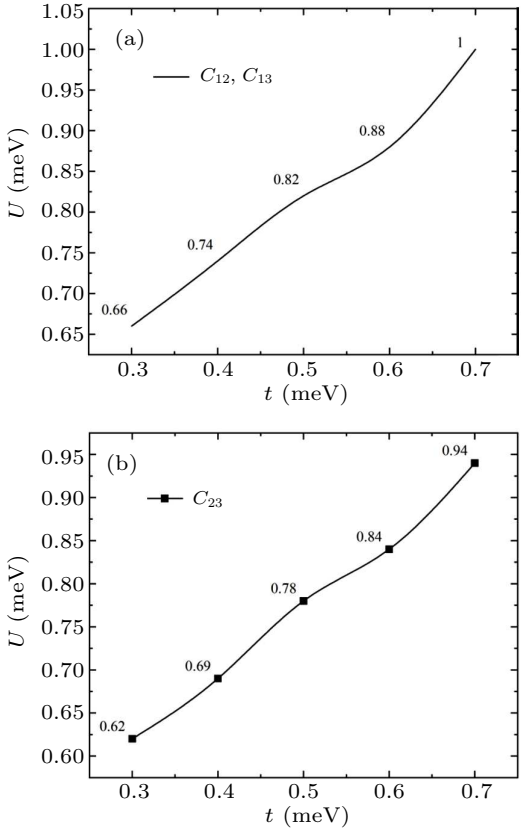


Fig. 5. (a) and (b) The relationship between t and U on the premise that concurrence reaches 0.9, which can be approximated as a linear relationship between t and U.

4. Implementation of the Toffoli quantum gate

In this part, the realization of the Toffoli gate under TTQDs is presented. The three qubits required for the Toffoli gate correspond to three quantum dots in the triangle. In order to better control the Toffoli quantum gate through the coupling between the applied magnetic field and the quantum dots, the Toffoli quantum gate is decomposed into multiple single-bit gates and double-bit gates. We operate within the computational basis of a three-qubit Hilbert space, which is spanned by the following eight orthonormal basis states:[39]

$$\{|000\rangle,\ |001\rangle,\ |010\rangle,\ |011\rangle,\ |100\rangle,\ |101\rangle,\ |110\rangle,\ |111\rangle\}.$$

The Toffoli quantum gate matrix has the following form:

$$U_{\text{Toffoli}} = \begin{bmatrix} 1 & 0 & 0 & 0 & 0 & 0 & 0 & 0 \\ 0 & 1 & 0 & 0 & 0 & 0 & 0 & 0 \\ 0 & 0 & 1 & 0 & 0 & 0 & 0 & 0 \\ 0 & 0 & 0 & 1 & 0 & 0 & 0 & 0 \\ 0 & 0 & 0 & 0 & 1 & 0 & 0 & 0 \\ 0 & 0 & 0 & 0 & 0 & 1 & 0 & 0 \\ 0 & 0 & 0 & 0 & 0 & 0 & 0 & 1 \\ 0 & 0 & 0 & 0 & 0 & 0 & 1 & 0 \end{bmatrix}.$$

Figure 6 presents the decomposition of the Toffoli gate into elementary quantum operations, including the CNOT gate, Hadamard (H) gate, T gate, and $T^{\dagger}$ gate.

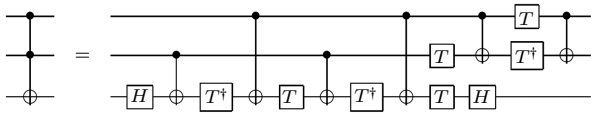


Fig. 6. The Toffoli gate[42] can be represented as a combination of a CNOT gate, T gate, $T^\dagger$ gate and H gate.

We first analyze how to implement the CNOT quantum gate. The function of the CNOT gate is to achieve controlled operations between quantum bits through conditional inversion. Figure 7[39] shows the implementation scheme of the CNOT gate based on the $\sqrt{\text{SWAP}}$ gate and single-qubit rotation. As shown in Fig. 7, we use a magnetic field[34–38] to regulate single qubit to achieve rotation operation $(R_x(\theta), R_y(\theta), R_z(\theta))$ and the use of spin coupling between quantum dots to achieve $\sqrt{\text{SWAP}}$ operation. With $R_x(\theta), R_y(\theta), R_z(\theta)$ and $\sqrt{\text{SWAP}}$ we can implement the CNOT operation.

The matrix form of $R_x(\theta), R_y(\theta), R_z(\theta)$ is expressed as

$$R_x(\theta) = \begin{bmatrix} \cos\frac{\theta}{2} & -\mathrm{i}\sin\frac{\theta}{2} \\ -\mathrm{i}\sin\frac{\theta}{2} & \cos\frac{\theta}{2} \end{bmatrix},$$

$$R_y(\theta) = \begin{bmatrix} \cos\frac{\theta}{2} & -\sin\frac{\theta}{2} \\ \sin\frac{\theta}{2} & \cos\frac{\theta}{2} \end{bmatrix},$$

$$R_z(\theta) = \begin{bmatrix} \mathrm{e}^{\frac{-\mathrm{i}\theta}{2}} & 0 \\ 0 & \mathrm{e}^{\frac{\mathrm{i}\theta}{2}} \end{bmatrix},$$

where θ represents the angle of rotation, with a range of $[-\pi, \pi]$. For single-qubit rotation, we can regulate by applying a magnetic field, according to the right-hand rule:[40,41] the right index finger points to the direction of the electron spin, the thumb points to the direction of the movement of electron spin, then the direction of the middle finger is the direction of the desired magnetic field.

When a magnetic field is applied to a single quantum dot, the Hamiltonian $H_1 = -\gamma B(t) \cdot S$, γ is the gyromagnetic ratio, and S is the spin operator. For the rotation operator for a single quantum dot, we represent it by the time evolution operator $U_R(\theta) = \mathrm{e}^{\gamma \int_0^{t_t} \mathrm{i} \cdot B \cdot S \,\mathrm{d}t}$, with $\int_0^t B \,\mathrm{d}t = \pi$, then the rotation matrix containing time can be obtained. When $B = 1$ T, it takes about π picoseconds to rotate $\pi/2$, and in Fig. 7, the time of these rotation operators can be obtained.

To complete the SWAP operation between two quantum dots, and the Hamiltonian of these two dots is $H_0 = J(t)\overrightarrow{S_i} \cdot \overrightarrow{S_{i+1}}$. The matrix form of the Hamiltonian is $\frac{1}{4}\hbar^2 J(t)(\sigma_x \otimes \sigma_x + \sigma_y \otimes \sigma_y + \sigma_z \otimes \sigma_z)$,where σ_x, σ_y, and σ_z represent the Pauli matrix respectively. The J is the Heisenberg commutative interaction $(J = 4t_{12}^2/U)$. The matrix U_{SWAP} of gate SWAP is obtained by the Hamiltonian H_0, $U_{\text{SWAP}}(t) = \mathrm{e}^{\int_0^t \mathrm{i} H_0 \,\mathrm{d}t}$, with $\int_0^t J \,\mathrm{d}t = \pi$. As evidenced in Fig. 4, the interdot concurrence maintains a significantly high value at the parameter configuration ($t = 1$ and $U = 1$), so when $t = 1$ and $U = 1$, we can get the SWAP implementation time of about $\pi/4$ ps. The matrix of U_{SWAP} is expressed as

$$U_{\text{SWAP}} = \begin{bmatrix} 1 & 0 & 0 & 0 \\ 0 & 0 & 1 & 0 \\ 0 & 1 & 0 & 0 \\ 0 & 0 & 0 & 1 \end{bmatrix}.$$

Now evolve the time to $\pi/8$ ps, then $\sqrt{\text{SWAP}}$ is obtained, and the matrix of $\sqrt{\text{SWAP}}$ is expressed as

$$U_{\sqrt{\text{SWAP}}} = \begin{bmatrix} 1 & 0 & 0 & 0 \\ 0 & \frac{1+\mathrm{i}}{2} & \frac{1-\mathrm{i}}{2} & 0 \\ 0 & \frac{1-\mathrm{i}}{2} & \frac{1+\mathrm{i}}{2} & 0 \\ 0 & 0 & 0 & 1 \end{bmatrix}.$$

From Fig. 7, we can calculate that it takes $21\pi/4$ ps to complete the complete CNOT quantum gate.

Next, we introduce the H gate, its matrix form is

$$H = \begin{bmatrix} \frac{1}{\sqrt{2}} & \frac{1}{\sqrt{2}} \\ \frac{1}{\sqrt{2}} & \frac{-1}{\sqrt{2}} \end{bmatrix}.$$

The operation of gate H corresponds to rotating $\pi/2$ around the y-axis and then π around the x-axis on the Bloch sphere, and the rotation operation can be achieved by magnetic field control. The time of the two actions is about 3π ps.

The matrix forms of the T and $T^\dagger$ gates are

$$T = \begin{bmatrix} 1 & 0 \\ 0 & \mathrm{e}^{\frac{\mathrm{i}\pi}{4}} \end{bmatrix}, \quad T^\dagger = \begin{bmatrix} 1 & 0 \\ 0 & \mathrm{e}^{\frac{-\mathrm{i}\pi}{4}} \end{bmatrix}.$$

The T and $T^\dagger$ gates represent a rotation of $\pi/4$ and $-\pi/4$ about the z-axis, respectively. The rotation operation can be achieved by magnetic field control. The time of the action is about $\pi/2$ ps.

In Fig. 6, the execution time for each operational step is explicitly calculated above, yielding a total gate operation time of 37π ps.

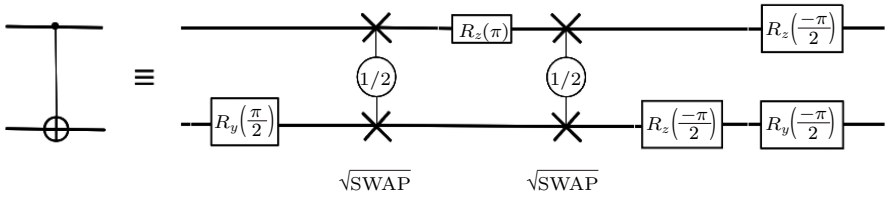


Fig. 7. The CNOT gate[39] can be represented as a combination of rotation operations $R_y(\theta), R_z(\theta)$ and the $\sqrt{\text{SWAP}}$ gate.

5. Conclusion

In this paper, we present a comprehensive investigation of quantum entanglement in TTQD systems. Our analysis systematically examines four critical parameters governing entanglement dynamics: interdot coupling strength t, Coulomb interaction U, temperature T, and electrode coupling Γ. Through comparative studies with a parallel triple quantum dot structure, we demonstrate that the triangular geometry exhibits significantly enhanced concurrence under identical conditions, attributed to its inherent geometric frustration and optimized quantum interference pathways. Numerical simulations further reveal a robust parameter regime for sustaining high entanglement (concurrence ≥ 0.9). These findings establish the triangular structure as a superior architecture for entanglement generation and provide concrete guidelines for experimental realization of tunable entangled states in semiconductor quantum dot platforms.

Finally, we theoretically demonstrate the implementation of three-qubit quantum gates within a TTQD architecture. Through detailed analysis of the system dynamics, we present a complete realization scheme for the Toffoli gate, including its decomposition into native operations and the corresponding pulse sequences. Numerical simulations of the gate operation yield a total execution time of 37 ps, demonstrating the potential for high-speed quantum operations in this configuration. This result suggests that the triangular quantum dot structure could serve as a viable platform for scalable multi-qubit quantum information processing.

Appendix A

When there is exactly one electron on each of the two quantum dots (referred to as the $(1,1)$ subspace), concurrence[33,43] can be expressed as

$$C_{ij}(t_t) = \max\left\{0, -\frac{1}{2} - 2\langle \overrightarrow{S_i}, \overrightarrow{S_j}\rangle\right\}, \tag{A1}$$

where $N_i^s = n_{i\uparrow} + n_{i\downarrow} - 2n_{i\uparrow}n_{i\downarrow}$, N_i^s represents the projection operator indicating the presence of a single electron on the QDi.

The subspace projection operator is constructed as $P = N_i^s N_j^s$, when quantum state $|\Psi(t_t)\rangle$ is projected onto the $(1,1)$ subspace, the normalized quantum state becomes

$$|\Psi_{(1,1)}(t_t)\rangle = \frac{N_i^s N_j^s |\Psi(t_t)\rangle}{\sqrt{\langle\Psi(t_t)|\overrightarrow{S_i}\cdot\overrightarrow{S_j}|\Psi(t_t)\rangle}}. \tag{A2}$$

In the normalized subspace, the expected value of the spin dot product is

$$\begin{aligned}\langle \overrightarrow{S_i}, \overrightarrow{S_j}\rangle_{(1,1)} &= \frac{\langle\Psi(t_t)|\langle\overrightarrow{S_i}\cdot\overrightarrow{S_j}N_i^s N_j^s|\Psi(t_t)\rangle}{\langle\Psi(t_t)|N_i^s N_j^s|\Psi(t_t)\rangle} \\ &= \frac{S_{ij}(t)}{\langle\Psi(t_t)|N_i^s N_j^s|\Psi(t_t)\rangle}.\end{aligned} \tag{A3}$$

Through substitution of formula (A3) into formula (A1), we obtain the resultant expression

$$C_{ij}(t_t) = \max\left\{0, -\frac{1}{2} - 2\frac{S_{ij}(t_t)}{\langle\Psi(t_t)|N_i^s N_j^s|\Psi(t_t)\rangle}\right\}. \tag{A4}$$

Acknowledgements

This work is supported by the National Natural Science Foundation of China (Grant Nos. 12274454, 11774418, 11374363, 11674317, 11974348, 11834014, and 21373191), the Strategic Priority Research Program of CAS (Grant Nos. XDB28000000 and XDB33000000), the Training Program of Major Research Plan of the National Natural Science Foundation of China (Grant No. 92165105), the Outstanding Innovative Talents Cultivation Funded Programs 2023 of Renmin University of China, the Fundamental Research Funds for the Central Universities, and the Research Funds of Renmin University of China. The computational resources have been provided by the Physical Laboratory of High Performance Computing at Renmin University of China.

References

[1] Chen K, Albeverio S and Fei S M 2005 *Phys. Rev. Lett.* **95** 040504
[2] Mintert F, Marek K and Buchleitner A 2006 *Phys. Rev. Lett.* **95** 260502
[3] Uhlmann A 2000 *Phys. Rev. A* **62** 032307
[4] Rafsanjani S M H, Huber M, Broadbent C J and Eberly J H 2012 *Phys. Rev. A* **86** 062303
[5] Majtey A P, Bouvrie P A, Valdes-Hernandez A and Plastino A R 2016 *Phys. Rev. A* **93** 032335
[6] Akhtarshenas S J 2010 *Phys. Rev. A* **83** 042306
[7] Yugra Y, Montenegro C and Zela F D 2022 *Phys. Rev. A* **105** 063710
[8] Walborn S P, Souto Ribeiro P H, Davidovich L, Mintert F and Buchleitner A 2006 *Nature* **440** 1022
[9] Krueger O and Werner R F 2005 *Physics* **99** 425
[10] Barnett S M and Phoenix S J D 1991 *Phys. Rev. A* **44** 535
[11] Buzek, Vladimir, Braunstein, S L and Hillery M 2000 *Phys. Rev. A* **63** 052313
[12] Kastoryano M J, Reiter F and Sorensen A S 2011 *Phys. Rev. Lett.* **106** 090502
[13] Levine H, Keesling A, Omran A, Bernien H, Schwartz S and Zibrov A S 2018 *Phys. Rev. Lett.* **121** 123603
[14] Pan J W, Daniell M, Gasparoni S, Weihs G and Zeilinger A 2001 *Phys. Rev. Lett.* **86** 4435
[15] Olivares S and Paris M G A 2011 *Phys. Rev. Lett.* **107** 170505
[16] Inamori H, Rallan L and Vedral V 2001 *J. Phys. A: Gen. Phys.* **34** 6913
[17] Zhang Z, Mower J, Englund D, Wong F N C and Shapiro J H 2014 *Phys. Rev. Lett.* **112** 120506
[18] Devetak I 2006 *Phys. Rev. Lett.* **97** 140503
[19] Buhrman H, Christandl M, Perry C and Zuiddam J 2016 *Phys. Rev. Lett.* **117** 230503
[20] Liu Y, Ju L, Liang X L, Tang S B, Tu G L S and Zhou L 2012 *Phys. Rev. Lett.* **109** 030501
[21] Portella-Oberli M T, Ciulin V, Berney J H, Deveaud B and Wojtowicz T 2012 *Phys. Rev. B* **69** 235311
[22] Gagliano E R and Balseiro C A 1988 *Phys. Rev. B* **38** 11766
[23] Slagle K, Bi Z, You Y Z and Xu C 2017 *Phys. Rev. B* **95** 165136
[24] Hu J, Luo M, Jiang F, Xu R X and Yan Y J 2011 *J. Chem. Phys.* **134** 101106
[25] Li Z H, Tong N H, Zheng X, Hou D, Wei J H and Hu J 2012 *Phys. Rev. Lett.* **109** 266403
[26] Wang Y D, Zhu Z G, Wei J H and Yan Y J 2020 *Eruophys. Lett.* **130** 17003
[27] Kehrein S K and Mielke A 1996 *Ann. Phys.* **252** 1

[28] Anders F B, Lebanon E and Schiller A 2004 *Phys. Rev. B* **70** 201306(R)
[29] Cheng Y X, Wang Y D, Wei J H, Zhu Z G and Yan Y J 2017 *Phys. Rev. B* **95** 155417
[30] Wang Y D, Ni J H and Wei J H 2017 *Phys. Rev. B* **96** 245426
[31] Weymann I, Bulka B R and Barnas J 2011 *Phys. Rev. B* **83** 113306
[32] Cheng Y X, Hou W J, Wang Y D, Li Z H, Wei J H and Yan Y J 2015 *New. J. Phys.* **17** 33009
[33] Busser C A and Heidrich-Meisner F 2013 *Phys. Rev. Lett.* **111** 246807
[34] Ishiwata S, Taguchi Y, Murakawa H, Onose Y and Tokura Y 2008 *Science* **319** 1643
[35] Brandt and Helmut E 1996 *Phys. Rev. B* **54** 4246
[36] Jouravlev O N and Nazarov Y V 2006 *Phys. Rev. Lett.* **96** 176804
[37] Ashoori R C, Stormer H L, Weiner J S, Pfeiffer L N, Baldwin K W and West K W 1993 *Phys. Rev. Lett.* **71** 613
[38] Liang C T, Simmons M Y, Smith C G, Kim G H, Ritchie D A and Pepper M 2012 *Phys. Rev. Lett.* **81** 3507
[39] Williams C P 2011 *Explorations in Quantum Computing* (Santa Clara, CA, United States) pp.99
[40] Griffiths D J 2013 *Introduction to Electrodynamics* 4th Ed. (Pearson)
[41] Hanson R, Kouwenhoven L P, Petta J R, Tarucha S and Vandersypen L M K 2007 *Rev. Mod. Phys.* **79** 1217
[42] Shende V V and Markov I L 2009 *Quantum. Inf. Comput.* **9** 461
[43] Wang X and Zanardi P 2002 *Phys. Rev. A* **301** 1
[44] Qi Y and Wei J H 2024 *Chin. Phys. B* **33** 57301
[45] Qi Y, Liu Y M, Wang Y D, Wei J H and Zhu Z G 2023 *Chin. Phys. B* **32** 087304